On rotation of frames and physical vectors: an exercise based on plate tectonics theory

Tomás Soler[a*], Jen-Yu Han[b]

[a]Spatial Reference System Division, National Geodetic Survey, NOAA, Silver Spring, MD 20910, USA
[b]Department of Civil Engineering, National Taiwan University, No. 1, Sect. 4, Roosevelt Road, Taipei 10617, Taiwan
[*]Corresponding author: E-mail: tom.soler@noaa.gov.

Abstract

The mathematical interaction between the simultaneous rotation of both a coordinate frame and a set of physical vectors in that frame is covered and theoretically and empirically explained. A practical example related to the secular motion of the pole is addressed. A least-squares adjustment is introduced to determine a possible displacement of the geodetic north pole of the frame caused by plausible changes in the coordinates of the observing stations defining the frame due to the rotation of the plates on which these stations are located. Two GPS network examples are investigated using the latest definition of the IGS08 geodetic frame, which was obtained exclusively using GPS data, as published by the International GNSS Service (IGS). The first network is the global GPS/IGS network, and the second one is a GPS/ILS-type single latitude network. The results of this exercise hints at the possibility that the secular global rotation of the frame caused by plate rotations should be accounted for in order to rigorously determine the true velocities of the rotation of the plates.

Introduction

The earth is formed by a group of rigid or quasi-rigid crustal tectonic plates moving individually with time. Consequently, geodetic reference frames are materialized by the coordinates of a set of core stations at a certain epoch and their corresponding linear velocities. Therefore, the residual changes of the three-dimensional position of these fiducial stations with time could introduce a small but detectable virtual secular motion of the reference frame itself. In this paper the angular variation with respect to time of the axes of the currently adopted geodetic reference frame due to plate rotations is investigated. Historically, the secular (non-periodic) angular displacement with respect to time of the z-axis of the frame (the so-called terrestrial motion of the CIP ≡ "Celestial Intermediate Pole", see Petit and Luzum 2010, p. 174) has been termed "secular motion of the pole." To quantify the secular motion of the pole produced by the displacement of the frame defining stations due to plate motions, the most recent GPS-determined geodetic frame was used. The International GNSS Service (IGS), every now and then, produces geodetic reference frames based on a set of global stations observing 24/7 the GPS constellation of satellites. The latest released frame of the series is the IGS08 (for the year/epoch 2005) and it is based on a set of 231 core stations where the (x, y, z) coordinates and their associated (v_x, v_y, v_z) velocities are accurately known.

The first aim of this exercise will be to determine what would be the secular motion of the polar axis of the IGS08 frame e.g. during a period of 50 years as a consequence of the displacements with time of the points defining the frame due to the rotation of the plates on which they are located. A least-squares (LS) procedure was introduced to rigorously determine the angular rotations of the secular motion and their corresponding variance-covariance (v-c) matrix. Thereafter, these angular values are converted into linear units to visualize the actual displacement on the earth's surface of the CIP and the Terrestrial Intermediate Origin (TIO, the origin of longitudes, see Petit and Luzum 2010, p. 179).

The difference between active and passive rotations is then addressed complementing the theoretical framework with a practical example based on the effect of plate tectonics on the core points defining the geodetic frame.

Subsequently, the Euler pole generated by these global rotations is determined and its secular contribution to the plate rotation velocity field quantified.

Secular motion of the pole caused by the motion of the observing stations

Assume that the original coordinates of the IGS08 core stations are denoted by (x, y, z). Then, after 50 years the value of the new coordinates $(\tilde{x}, \tilde{y}, \tilde{z})$ could be written as:

$$\{\tilde{x}\} = \{x\} + \{dx\}; \quad \begin{Bmatrix} \tilde{x} \\ \tilde{y} \\ \tilde{z} \end{Bmatrix} = \begin{Bmatrix} x \\ y \\ z \end{Bmatrix} + \begin{Bmatrix} dx \\ dy \\ dx \end{Bmatrix} = \begin{Bmatrix} x \\ y \\ z \end{Bmatrix} + \begin{Bmatrix} v_x \\ v_y \\ v_z \end{Bmatrix}(t - t_0) = \{x\} + \{v\}dt \tag{1}$$

where, for this particular exercise, $t - t_0 = dt = 50$ years.

The mathematical model required to compute the angular displacements of the pole after 50 years, assuming differential rotations, is simplified as (see Soler 1998):

$$\{\tilde{x}\}_i = \mathbf{R}_3(\delta\alpha_3)\mathbf{R}_2(\delta\alpha_2)\mathbf{R}_1(\delta\alpha_1)\{x\}_i = \delta\mathbf{R}\{x\}_i = \square[1] + [\underline{\delta\alpha}]^T \square\{x\}_i = \begin{bmatrix} 1 & \delta\alpha_3 & -\delta\alpha_2 \\ -\delta\alpha_3 & 1 & \delta\alpha_1 \\ \delta\alpha_2 & -\delta\alpha_1 & 1 \end{bmatrix} \begin{Bmatrix} x \\ y \\ z \end{Bmatrix}_i \tag{2}$$

The above equation has implicitly two assumptions: 1) the three rotations $\delta\alpha_1, \delta\alpha_2, \delta\alpha_3$ respectively about the three original Cartesian axes (x, y, z) are differentially small, and 2) counterclockwise (anticlockwise) rotations about the three axes are positive. The letter i is an index identifying the station in question. The general form of the proper orthogonal rotation matrices of the form $\mathbf{R}_j(\theta)$, $j = 1, 2, 3$ materializing a counterclockwise rotation of coordinate axis was given in Kaula (1966; p. 13). The rotation matrix subscripts indicate rotations about the first, second, and third axis, respectively. The angular argument θ represents the magnitude of the rotation, which can be any finite angle. Explicit matrix forms of each representative counterclockwise rotation of an angle θ about each one of the three axes are well known (Mueller 1969, p. 80). Successive rotations are operated in a sequential manner from right to left. Generally, the product of two or more rotation matrices is not commutative, however, the arguments of the rotations contained in (2) are differentially small and in this particular case they fulfill the commutative law. Therefore, one can write, assuming all possibilities:

$$\left.\begin{array}{l}\mathbf{R}_3(\delta\alpha_3)\mathbf{R}_2(\delta\alpha_2)\mathbf{R}_1(\delta\alpha_1)\\ \mathbf{R}_2(\delta\alpha_2)\mathbf{R}_1(\delta\alpha_1)\mathbf{R}_3(\delta\alpha_3)\\ \mathbf{R}_1(\delta\alpha_1)\mathbf{R}_3(\delta\alpha_3)\mathbf{R}_2(\delta\alpha_2)\\ \mathbf{R}_1(\delta\alpha_1)\mathbf{R}_2(\delta\alpha_2)\mathbf{R}_3(\delta\alpha_3)\\ \mathbf{R}_2(\delta\alpha_2)\mathbf{R}_3(\delta\alpha_3)\mathbf{R}_1(\delta\alpha_1)\\ \mathbf{R}_3(\delta\alpha_3)\mathbf{R}_1(\delta\alpha_1)\mathbf{R}_2(\delta\alpha_2)\end{array}\right\}=\begin{bmatrix}1 & \delta\alpha_3 & -\delta\alpha_2\\ -\delta\alpha_3 & 1 & \delta\alpha_1\\ \delta\alpha_2 & -\delta\alpha_1 & 1\end{bmatrix}=\delta\mathbf{R} \tag{3}$$

Notice that (2) implies that an arbitrary point P remains fixed in space while one set of axes is rotated counterclockwise by amounts $\delta\alpha_1, \delta\alpha_2, \delta\alpha_3$. Figure 1 shows that although the point remains fixed in space its coordinates before and after the rotations are different; $\{x\}$ is the column vector of coordinates before the rotation and $\{\tilde{x}\}$ is the column vector of coordinates after the rotation referred to the new rotated frame $(\tilde{x}, \tilde{y}, \tilde{z})$. As the figure indicates both sets of coordinates apply to the same point P which remains fixed in space.
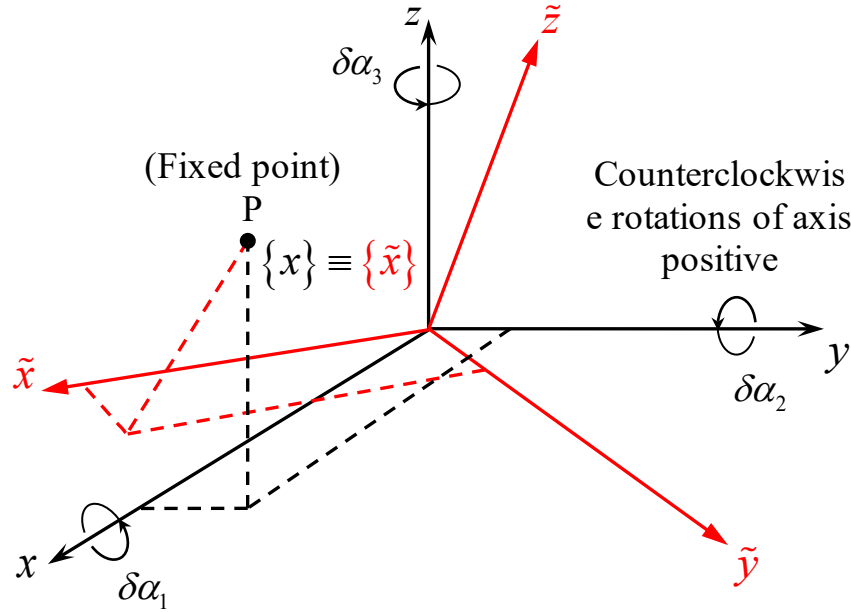

Fig. 1 Coordinates of a fixed point P in space before and after a frame rotation

From (2) immediately follows that the differential changes to the original coordinates due to a differential counterclockwise rotation of axes are:

$$\left\{\begin{array}{c}\delta x\\ \delta y\\ \delta z\end{array}\right\}_i=\begin{bmatrix}0 & \delta\alpha_3 & -\delta\alpha_2\\ -\delta\alpha_3 & 0 & \delta\alpha_1\\ \delta\alpha_2 & -\delta\alpha_1 & 0\end{bmatrix}\left\{\begin{array}{c}x\\ y\\ z\end{array}\right\}_i=[\underline{\delta\alpha}]^T\{x\}_i \tag{4}$$

4

Consequently, if one is given a set of three rotations $\delta\alpha_1, \delta\alpha_2, \delta\alpha_3$ and wants to compute the differential effect due to three clockwise rotations about the same three axes, equation (4) takes the form:

$$\begin{Bmatrix} \delta\bar{x} \\ \delta\bar{y} \\ \delta\bar{z} \end{Bmatrix}_i = \begin{bmatrix} 0 & -\delta\alpha_3 & \delta\alpha_2 \\ \delta\alpha_3 & 0 & -\delta\alpha_1 \\ -\delta\alpha_2 & \delta\alpha_1 & 0 \end{bmatrix} \begin{Bmatrix} x \\ y \\ z \end{Bmatrix}_i = [\delta\alpha]\{x\}_i \tag{5}$$

were $\delta\bar{x}$, $\delta\bar{y}$, and $\delta\bar{z}$ are the displacements of the point due to a clockwise rotation. Clearly, in this case, $\delta\bar{x} = -\delta x$, $\delta\bar{y} = -\delta y$, and $\delta\bar{z} = -\delta z$.

Least-squares procedure to determine $\delta\alpha_1, \delta\alpha_2$ and $\delta\alpha_3$

Equation (2) could be explicitly written:

$$\begin{Bmatrix} \tilde{x} \\ \tilde{y} \\ \tilde{z} \end{Bmatrix}_i = \begin{Bmatrix} x + \delta\alpha_3 y - \delta\alpha_2 z \\ -\delta\alpha_3 x + y + \delta\alpha_1 z \\ \delta\alpha_2 x - \delta\alpha_1 y + z \end{Bmatrix}_i \tag{6}$$

Using a least-squares methodology, the above expression conforms with a general implicit or mixed model of the type $F(L, X) = 0$ where the symbol L denotes observations and X parameters or, equivalently, unknowns (see Leick 1995, p. 116). Therefore, equation (6) expressed as an implicit functional relationship, assuming $i = 1, 2, 3 \ldots n$, where n denotes the total number of points used in the analysis takes the following form:

$$\begin{aligned}
F_1 &: x_1 + \delta\alpha_3 y_1 - \delta\alpha_2 z_1 - \tilde{x}_1 = 0 \\
F_2 &: -\delta\alpha_3 x_1 + y_1 + \delta\alpha_1 z_1 - \tilde{y}_1 = 0 \\
F_3 &: \delta\alpha_2 x_1 - \delta\alpha_1 y_1 + z_1 - \tilde{z}_1 = 0 \\
&\qquad\qquad \vdots \\
F_{3n-2} &: x_n + \delta\alpha_3 y_n - \delta\alpha_2 z_n - \tilde{x}_n = 0 \\
F_{3n-1} &: -\delta\alpha_3 x_n + y_n + \delta\alpha_1 z_n - \tilde{y}_n = 0 \\
F_{3n} &: \delta\alpha_2 x_n - \delta\alpha_1 y_n + z_n - \tilde{z}_n = 0
\end{aligned} \tag{7}$$

But according to (1),

$$\tilde{x}_i = x_i + v_{x_i} dt$$
$$\tilde{y}_i = y_i + v_{y_i} dt \tag{8}$$
$$\tilde{z}_i = z_i + v_{z_i} dt$$

Therefore, substituting (8) into (7) one finally arrives at:

$$F_1: \quad \delta\alpha_3 y_1 - \delta\alpha_2 z_1 - v_{x_1} dt = 0$$
$$F_2: \quad -\delta\alpha_3 x_1 + \delta\alpha_1 z_1 - v_{y_1} dt = 0$$
$$F_3: \quad \delta\alpha_2 x_1 - \delta\alpha_1 y_1 - v_{z_1} dt = 0$$
$$\vdots \tag{9}$$
$$F_{3n-2}: \quad \delta\alpha_3 y_n - \delta\alpha_2 z_n - v_{x_n} dt = 0$$
$$F_{3n-1}: \quad -\delta\alpha_3 x_n + \delta\alpha_1 z_n - v_{y_n} dt = 0$$
$$F_{3n}: \quad \delta\alpha_2 x_n - \delta\alpha_1 y_n - v_{z_n} dt = 0$$

Clearly, the three unknowns that one wants to estimate are the counterclockwise differential rotations $\delta\alpha_1, \delta\alpha_2, \delta\alpha_3$ around the three (x, y, z) axes, respectively. The two sets of observation vectors at our disposal are the original coordinates of the points $\{x\ y\ z\}_i^T$ and the corresponding linear site velocities at each point $\{v_x\ v_y\ v_z\}_i^T$ at one given epoch.

The design matrix $\mathbf{A}$ is computed according to the following well-known matrix expression that contains the partial derivatives with respect to three parameters p, in this particular case, $p_1 = \delta\alpha_1$, $p_2 = \delta\alpha_2$, and $p_3 = \delta\alpha_3$:

$$\mathbf{A}_{3n \times 3} = \frac{\partial F}{\partial X}\Big|_{X_0, L_b} = \left\{ \begin{bmatrix} \dfrac{\partial F_1}{\partial p_1} & \dfrac{\partial F_1}{\partial p_2} & \dfrac{\partial F_1}{\partial p_3} \\[2mm] \dfrac{\partial F_2}{\partial p_1} & \dfrac{\partial F_2}{\partial p_2} & \dfrac{\partial F_2}{\partial p_3} \\[2mm] \dfrac{\partial F_3}{\partial p_1} & \dfrac{\partial F_3}{\partial p_2} & \dfrac{\partial F_3}{\partial p_3} \end{bmatrix}_1 \\ \vdots \\ \begin{bmatrix} \dfrac{\partial F_{3n-2}}{\partial p_1} & \dfrac{\partial F_{3n-2}}{\partial p_2} & \dfrac{\partial F_{3n-2}}{\partial p_3} \\[2mm] \dfrac{\partial F_{3n-1}}{\partial p_1} & \dfrac{\partial F_{3n-1}}{\partial p_2} & \dfrac{\partial F_{3n-1}}{\partial p_3} \\[2mm] \dfrac{\partial F_{3n}}{\partial p_1} & \dfrac{\partial F_{3n}}{\partial p_2} & \dfrac{\partial F_{3n}}{\partial p_3} \end{bmatrix}_n \right\} = \left\{ \begin{bmatrix} 0 & -z_1 & y_1 \\ z_1 & 0 & -x_1 \\ -y_1 & x_1 & 0 \end{bmatrix} \\ \vdots \\ \begin{bmatrix} 0 & -z_n & y_n \\ z_n & 0 & -x_n \\ -y_n & x_n & 0 \end{bmatrix} \right\} \tag{10}$$

where X_0, L_0, indicates the initial values for the parameters and the observations, respectively. Similarly, the design matrix **B** is computed as:

$$\mathbf{B}_{3n \times 6n} = \frac{\partial F}{\partial L}\bigg|_{X_0, L_b}$$

$$= \begin{bmatrix}
\begin{bmatrix}
\frac{\partial F_1}{\partial x_1} & \frac{\partial F_1}{\partial y_1} & \frac{\partial F_1}{\partial z_1} & \frac{\partial F_1}{\partial v_{x_1}} & \frac{\partial F_1}{\partial v_{y_1}} & \frac{\partial F_1}{\partial v_{z_1}} \\
\frac{\partial F_2}{\partial x_1} & \frac{\partial F_2}{\partial y_1} & \frac{\partial F_2}{\partial z_1} & \frac{\partial F_2}{\partial v_{x_1}} & \frac{\partial F_2}{\partial v_{y_1}} & \frac{\partial F_2}{\partial v_{z_1}} \\
\frac{\partial F_3}{\partial x_1} & \frac{\partial F_3}{\partial y_1} & \frac{\partial F_3}{\partial z_1} & \frac{\partial F_3}{\partial v_{x_1}} & \frac{\partial F_3}{\partial v_{y_1}} & \frac{\partial F_3}{\partial v_{z_1}}
\end{bmatrix} & \cdots & \begin{bmatrix}
\frac{\partial F_1}{\partial x_n} & \frac{\partial F_1}{\partial y_n} & \frac{\partial F_1}{\partial z_n} & \frac{\partial F_1}{\partial v_{x_n}} & \frac{\partial F_1}{\partial v_{y_n}} & \frac{\partial F_1}{\partial v_{z_n}} \\
\frac{\partial F_2}{\partial x_n} & \frac{\partial F_2}{\partial y_n} & \frac{\partial F_2}{\partial z_n} & \frac{\partial F_2}{\partial v_{x_n}} & \frac{\partial F_2}{\partial v_{y_n}} & \frac{\partial F_2}{\partial v_{z_n}} \\
\frac{\partial F_3}{\partial x_n} & \frac{\partial F_3}{\partial y_n} & \frac{\partial F_3}{\partial z_n} & \frac{\partial F_3}{\partial v_{x_n}} & \frac{\partial F_3}{\partial v_{y_n}} & \frac{\partial F_3}{\partial v_{z_n}}
\end{bmatrix} \\
\vdots & \ddots & \vdots \\
\begin{bmatrix}
\frac{\partial F_{3n-2}}{\partial x_1} & \frac{\partial F_{3n-2}}{\partial y_1} & \frac{\partial F_{3n-2}}{\partial z_1} & \frac{\partial F_{3n-2}}{\partial v_{x_1}} & \frac{\partial F_{3n-2}}{\partial v_{y_1}} & \frac{\partial F_{3n-2}}{\partial v_{z_1}} \\
\frac{\partial F_{3n-1}}{\partial x_1} & \frac{\partial F_{3n-1}}{\partial y_1} & \frac{\partial F_{3n-1}}{\partial z_1} & \frac{\partial F_{3n-1}}{\partial v_{x_1}} & \frac{\partial F_{3n-1}}{\partial v_{y_1}} & \frac{\partial F_{3n-1}}{\partial v_{z_1}} \\
\frac{\partial F_{3n}}{\partial x_1} & \frac{\partial F_{3n}}{\partial y_1} & \frac{\partial F_{3n}}{\partial z_1} & \frac{\partial F_{3n}}{\partial v_{x_1}} & \frac{\partial F_{3n}}{\partial v_{y_1}} & \frac{\partial F_{3n}}{\partial v_{z_1}}
\end{bmatrix} & \cdots & \begin{bmatrix}
\frac{\partial F_{3n-2}}{\partial x_n} & \frac{\partial F_{3n-2}}{\partial y_n} & \frac{\partial F_{3n-2}}{\partial z_n} & \frac{\partial F_{3n-2}}{\partial v_{x_n}} & \frac{\partial F_{3n-2}}{\partial v_{y_n}} & \frac{\partial F_{3n-2}}{\partial v_{z_n}} \\
\frac{\partial F_{3n-1}}{\partial x_n} & \frac{\partial F_{3n-1}}{\partial y_n} & \frac{\partial F_{3n-1}}{\partial z_n} & \frac{\partial F_{3n-1}}{\partial v_{x_n}} & \frac{\partial F_{3n-1}}{\partial v_{y_n}} & \frac{\partial F_{3n-1}}{\partial v_{z_n}} \\
\frac{\partial F_{3n}}{\partial x_n} & \frac{\partial F_{3n}}{\partial y_n} & \frac{\partial F_{3n}}{\partial z_n} & \frac{\partial F_{3n}}{\partial v_{x_n}} & \frac{\partial F_{3n}}{\partial v_{y_n}} & \frac{\partial F_{3n}}{\partial v_{z_n}}
\end{bmatrix}
\end{bmatrix}$$

$$= \begin{bmatrix}
\begin{bmatrix}
0 & \delta\alpha_3 & -\delta\alpha_2 & -dt & 0 & 0 \\
-\delta\alpha_3 & 0 & \delta\alpha_1 & 0 & -dt & 0 \\
\delta\alpha_2 & -\delta\alpha_1 & 0 & 0 & 0 & -dt
\end{bmatrix}_1 & \cdots & \begin{bmatrix}
0 & 0 & 0 & 0 & 0 & 0 \\
0 & 0 & 0 & 0 & 0 & 0 \\
0 & 0 & 0 & 0 & 0 & 0
\end{bmatrix} \\
\vdots & \ddots & \vdots \\
\begin{bmatrix}
0 & 0 & 0 & 0 & 0 & 0 \\
0 & 0 & 0 & 0 & 0 & 0 \\
0 & 0 & 0 & 0 & 0 & 0
\end{bmatrix} & \cdots & \begin{bmatrix}
0 & \delta\alpha_3 & -\delta\alpha_2 & -dt & 0 & 0 \\
-\delta\alpha_3 & 0 & \delta\alpha_1 & 0 & -dt & 0 \\
\delta\alpha_2 & -\delta\alpha_1 & 0 & 0 & 0 & -dt
\end{bmatrix}_n
\end{bmatrix}$$

(11)

The so-called "closure vector" **W** takes the explicit form:

$$
\underset{3n\times1}{\mathbf{W}} = F(L_b, X_0) = \begin{Bmatrix} \delta\alpha_3^0 y_1 - \delta\alpha_2^0 z_1 - v_{x_1} dt \\ -\delta\alpha_3^0 x_1 + \delta\alpha_1^0 z_1 - v_{y_1} dt \\ \delta\alpha_2^0 x_1 - \delta\alpha_1 y_1 - v_{z_1} dt \\ \vdots \\ \delta\alpha_3^0 y_n - \delta\alpha_2^0 z_n - v_{x_n} dt \\ -\delta\alpha_3^0 x_n + \delta\alpha_1^0 z_n - v_{y_n} dt \\ \delta\alpha_2^0 x_n - \delta\alpha_1^0 y_n - v_{z_n} dt \end{Bmatrix} \tag{12}
$$

The quantities $\delta\alpha_1^0, \delta\alpha_2^0, \delta\alpha_3^0$ are the initial approximate values of the rotations that are been estimated. In this investigation all initial rotations were assumed to be equal to zero. The same values were used in (11). The solution converged after three iterations.

To compute the matrix $\mathbf{P}^{-1}$ required in any LS formalism (see (17)) one needs the v-c matrices of the original IGS08 observed coordinates and velocities, that is:

$$
\underset{6n\times6n}{\mathbf{P}^{-1}} = \frac{1}{\sigma_0^2} \begin{bmatrix} \begin{bmatrix} \underset{3\times3}{\Sigma_{x_1}} & \underset{3\times3}{\Sigma_{x_1 v_{x_1}}} \\ sym & \underset{3\times3}{\Sigma_{v_{x_1}}} \end{bmatrix} & \cdots & \begin{bmatrix} [0] & [0] \\ sym & [0] \end{bmatrix} \\ & \ddots & \vdots \\ & & \begin{bmatrix} \underset{3\times3}{\Sigma_{x_n}} & \underset{3\times3}{\Sigma_{x_n v_{x_n}}} \\ sym & \underset{3\times3}{\Sigma_{v_{x_n}}} \end{bmatrix} \\ sym & & \end{bmatrix} \tag{13}
$$

where the cross-correlations between coordinates and velocities of different stations was assumed to be equal to zero, namely:

$$
\Sigma_{x_i x_j} = \Sigma_{x_i v_{x_j}} = \Sigma_{v_{x_i} x_j} = \Sigma_{v_{x_i} v_{x_j}} = \underset{3\times3}{[0]} \qquad (i \neq j) \tag{14}
$$

The value of σ_0^2 is the a priori variance of unit weight that in this work was assumed equal to one. The required values of the matrices in (13) are given in the SINEX file provided by the IGS, however, they contain "formal statistics", also described as "formal errors", and therefore they

are perhaps slightly optimistic and not representative at a certain level of accuracy of the real behavior of the physical-geometric model involved in the GPS-processed multiyear solutions. Using similar reasoning to the one introduced in Soler et al. (2012) to scale optimistic stochastic models generally available to us in raw GPS SINEX files, the final value of the inverse of the weight matrix was modified as follows:

$$
\underset{6n\times6n}{\mathbf{P}^{-1}} = \frac{1}{\sigma_0^2}
\begin{bmatrix}
\begin{bmatrix} \underset{3\times3}{\mathbf{J}_x \boldsymbol{\Sigma}_{x_1} \mathbf{J}_x^T} & \underset{3\times3}{\mathbf{J}_x \boldsymbol{\Sigma}_{x_1 v_{x_1}} \mathbf{J}_v^T} \\ sym & \underset{3\times3}{\mathbf{J}_v \boldsymbol{\Sigma}_{v_{x_1}} \mathbf{J}_v^T} \end{bmatrix} & \cdots & \begin{bmatrix} [0] & [0] \\ sym & [0] \end{bmatrix} \\
& \ddots & \vdots \\
& & \begin{bmatrix} \underset{3\times3}{\mathbf{J}_x \boldsymbol{\Sigma}_{x_n} \mathbf{J}_x^T} & \underset{3\times3}{\mathbf{J}_x \boldsymbol{\Sigma}_{x_n v_{x_n}} \mathbf{J}_v^T} \\ sym & \underset{3\times3}{\mathbf{J}_v \boldsymbol{\Sigma}_{v_{x_n}} \mathbf{J}_v^T} \end{bmatrix} \\
& sym &
\end{bmatrix}
\tag{15}
$$

where:

$$
\underset{3\times3}{\mathbf{J}_x} = s_x \underset{3\times3}{\mathbf{I}} \quad \text{and} \quad \underset{3\times3}{\mathbf{J}_v} = s_v \underset{3\times3}{\mathbf{I}}
\tag{16}
$$

The two multipliers s_x and s_v used to scale the original v-c matrices of the coordinates and velocities were selected to be 200 and 350, respectively (see later the "Data used" section.) Then, using the standard least-squares methodology, to get the solution the following set of matrices was calculated (Leick 1995):

$$
\begin{aligned}
\mathbf{M} &= \mathbf{B}\mathbf{P}^{-1}\mathbf{B}^T \\
\mathbf{N} &= \mathbf{A}^T\mathbf{M}^{-1}\mathbf{A} \\
\mathbf{U} &= \mathbf{A}^T\mathbf{M}^{-1}\mathbf{W} \\
\hat{\mathbf{X}} &= -\mathbf{N}^{-1}\mathbf{U} \\
\mathbf{V} &= -\mathbf{P}^{-1}\mathbf{B}^T\mathbf{M}(\mathbf{W} - \mathbf{A}\hat{\mathbf{X}})
\end{aligned}
\tag{17}
$$

The v-c matrix for the estimated parameters and the a posteriori variance of unit weight can be obtained respectively by:

$$
\boldsymbol{\Sigma}_{\hat{X}} = \hat{\sigma}_0^2 \mathbf{N}^{-1} = \hat{\sigma}_0^2 (\mathbf{A}^T\mathbf{M}^{-1}\mathbf{A})^{-1}
\tag{18}
$$

where

$$\hat{\sigma}_0^2 = \frac{\mathbf{V}^T \mathbf{P} \mathbf{V}}{3n - 3} \qquad (19)$$

Relationship between angular and linear units to represent the displacements of the pole

Historically, the displacements around the north pole are represented using a local two-dimensional Cartesian frame denoted (x_p, y_p) (see Mueller 1969, p.82; McCarthy and Luzum 1996) where x_p and y_p are the so-called "polar coordinates" of the displaced (rotated) third axis of the IGS08 frame caused by the motion of the stations-- in the case at hand, assumed exclusively caused by plate rotations-- with respect to the position of the original IGS08 frame during the interval $dt = 50$ years. Incidentally, the value of dt could have been selected equal to one year. The results are linear and could have been extrapolated to a period of 50 years giving the same results. The selection interval of 50 years was mainly selected for cosmetic reasons in order to obtain final angular results larger than 1 mas (milliarcsecond). To convert the pole displacements from the computed angular units to linear units, one assumes the local frame on a plane tangent to the mean earth's geocentric ellipsoid (GRS80) at the point of intersection of the original IGS08 frame third-axis with this rotational ellipsoid. A comprehensive view of the angular relationship between the original $(x, y, z)_{IGS08}$ frame and the rotated $(\tilde{x}, \tilde{y}, \tilde{z})_{IGS08}$ frame is provided in Figure 2.
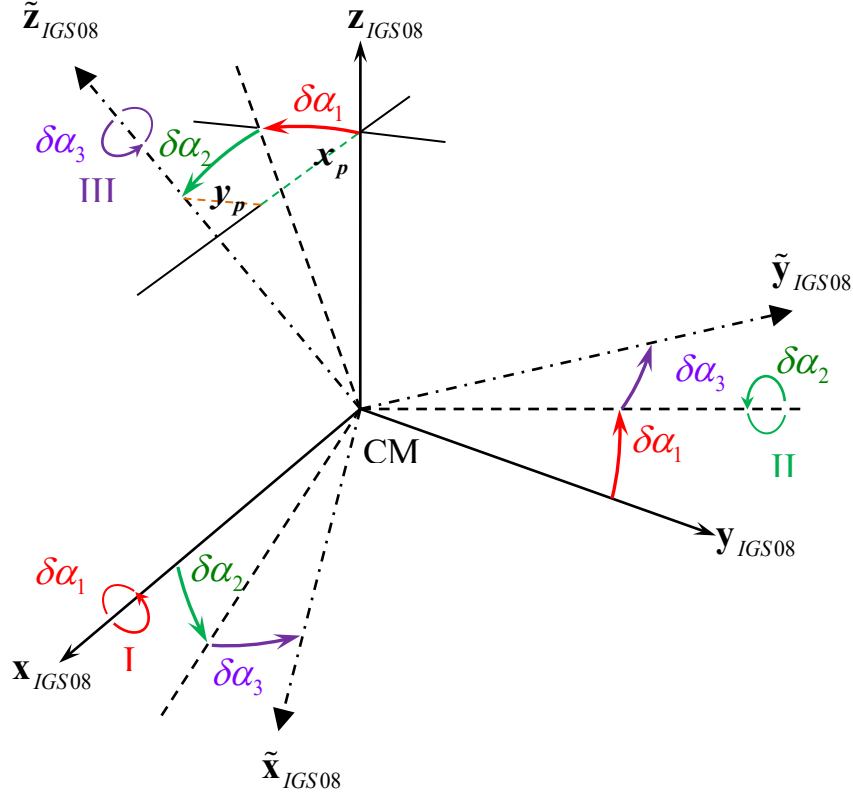
Fig. 2 Basic rotations between the frames $(x, y, z)_{IGS08}$ and $(\tilde{x}, \tilde{y}, \tilde{z})_{IGS08}$ caused by plate motions at the IGS08 core stations. The local linear coordinates x_p and y_p of the displaced polar axis are also shown. The figure is not drawn to scale. CM = earth's center of mass

Following the standard definition of the (x_p, y_p) local frame, that is, the axis x_p is parallel to the x_{IGS08} axis, represented symbolically by $x_p \square x_{IGS08}$ and, similarly, $y_p \square -y_{IGS08}$, the following equalities could be written:

$$\begin{Bmatrix} y_p \\ x_p \\ \lambda_p \end{Bmatrix} = \begin{bmatrix} M_{\varphi=90^0} & 0 & 0 \\ 0 & M_{\varphi=90^0} & 0 \\ 0 & 0 & N_{\varphi=0^0} \end{bmatrix} \begin{Bmatrix} \delta\alpha_1 \\ \delta\alpha_2 \\ \delta\alpha_3 \end{Bmatrix} = \mathbf{H}_{3\times3} \begin{Bmatrix} \delta\alpha_1 \\ \delta\alpha_2 \\ \delta\alpha_3 \end{Bmatrix} \tag{20}$$

In the above equation the value of λ_p indicates the approximate displacement in linear units along the earth's equator of the secular motion of the origin of longitudes. This approximation assumes that the equatorial plane of the initial IGS08 frame $(x, y, z)_{IGS08}$ is equal or very close to the equatorial plane defined by the rotated $(\tilde{x}, \tilde{y}, \tilde{z})_{IGS08}$ frame. The symbols M and N represent

the values of the principal radius of curvature along the meridian and prime vertical respectively, computed at the specified geodetic latitudes in (20) assuming a two-parameter ellipsoidal earth. These principal radii of curvature could be computed according to the well-known equations (see Soler et al. 2012):

$$M = \frac{a(1-e^2)}{W^3}; \quad N = \frac{a}{W}; \quad W^2 = 1 - e^2 \sin^2 \varphi; \quad e^2 = 2f - f^2 \tag{21}$$

In the above equations, a and f denote the semi-major axis and flattening of the selected reference ellipsoid, respectively. For all computations performed herein the so-called Geodetic Reference System ellipsoid of 1980 (GRS80) was adopted: a = 6,378,137 m, exact; $f \approx$ 1/298.257222101 (Moritz 1992).

The values of M and N particularized to the latitudes shown in (20) gives:

$$M_{\varphi=90^0} = \frac{a}{\sqrt{1-e^2}}; \quad N_{\varphi=0^0} = a \tag{22}$$

The results from (20) are more accurate that the standard procedure of assuming a spherical earth where $0.001" \approx 3\,cm$ on its surface. From (20) the full v-c matrix of the displacements of the pole (in linear units) as determined from recent GPS observations defining the IGS08 frame immediately follows:

$$\Sigma_{\{y_p, x_p, \lambda_p\}} = \mathbf{H}\Sigma_{\{\delta\alpha_1, \delta\alpha_2, \delta\alpha_3\}}\mathbf{H}^T = \mathbf{H}\Sigma_{\{\delta\alpha_1, \delta\alpha_2, \delta\alpha_3\}}\mathbf{H} \tag{23}$$

Data used

In this investigation the coordinates and velocities of the IGS08 core stations defining the IGS08 reference frame at epoch t_0 = 2005.000 were used as the starting values. The stochastic model, that is, the v-c matrices required in the diagonal blocks of (13) were extracted from the IGS08 SINEX file. The location of the IGS08 core stations are plotted in Figure 3 against the

Fig. 3 Circles and squares depict the 231 core stations defining the IGS08 geodetic frame. The closest IGS stations to the old ILS astronomical observatories are represented by squares

background of tectonic plates available at the URL: http://peterbird.name/publications/ 2003_PB2002/2003_PB2002.htm. To be discussed later, the figure also depicts the five stations from the IGS08 set closest to the astronomical observatories belonging to the now defunct International Latitude Service (ILS). The ILS was an international organization created in 1899 to monitor the complicated motion of the path of the instantaneous earth's axis of rotation on the surface of the earth (Höpfner 2000; Yokoyama et al. 2000). Using classical astronomical techniques, and zenith telescopes, five observatories located approximately on the same parallel (φ = 39º 08') determined the variation of latitude over time. The main reason why the observatories were selected along the same parallel was to assure, as much as possible, that any important systematic errors (e.g. errors in star catalogues, etc.) were common to all data processing methods performed at each observatory. At the time it was not known that the latitude of each station was affected by small variations due to the individual rotation of the plates. As a result of this effort the ILS produced a precise general plot of the wobble of the earth on its rotation axis (Chandlers' wobble) and even detected a still unexplained secular motion of the pole. These observatories ceased to operate in 1982 when new, more accurate, spatial geodetic techniques were developed and fully implemented. It should also be stressed that while the ILS was operational a comprehensive theory of lithospheric plate tectonics was not well known. In this investigation to recreate as much as possible a potential virtual secular motion of the pole

13

originated by the rotation of the plates at the ILS observatories, the IGS08 GPS-sites closest to the original ILS telescopes were also independently studied. Table 1 presents the approximate coordinates of the five IGS08 core stations closest to the ILS observatories that were used in this exercise tabulated by ascending longitude (positive towards east). As mentioned above, the actual geographic locations of these five IGS08 stations are depicted by squares in Figure 3.

Table 1 Coordinates of the five IGS08 core stations closest to the old ILS astronomical observatories. Longitude is assumed positive east

ILS Stations	Nearby IGS Station	Plate	Longitude (d-m-s)	Latitude (d-m-s)
CARLOFORTE (Italy)	CAGL	EU	08-58-21.91	39-08-09.28
KITAB (Russia)	KIT3	EU	66-53-07.60	39-08-05.16
MIZUSAWA (Japan)	TSKB	EU?	140-05-14.99	36-06-20.45
UKIAH (USA)	QUIN	NA	239-03-20.06	39-58-28.40
GAITHERSBURG (USA)	USN3	NA	282-56-01.41	38-55-14.03

The values of the coordinates $\{x\}$ and velocities $\{v\}$ of all core stations defining the IGS08 frame at epoch 2005.00 are given at the Web site ftp://igs-rf.ign.fr/pub/IGb08 under the file name IGb08.ssc. To see the data corresponding to the coordinates and velocities of the 231 core stations, scroll down in the file to "SOLUTION/ESTIMATE". Notice that under some station names may be several entries with coordinate values very close to each other; they are the result of various GPS solutions processed using different spans of time. For this investigation a unique set of (x, y, z) coordinates for each station was selected, the one containing the minimum standard deviations. Additionally, as mentioned earlier, the original v-c matrix (formal statistics) extracted from the SINEX file is usually too optimistic. Multipliers must be decided in order to scale the mostly optimistic stochastic model. As already was announced in Section 3, after (16), in this study, two multipliers $s_x = 200$ and $s_v = 350$ have been obtained empirically by constraining the *a posteriori* variance of unit weight to be close to unity. This will guarantee a much more reasonable stochastic model ensuing a more realistic uncertainty estimates for the determined parameters well in accordance with the proposed general least-squares approach.

Results using all available IGS08 stations

Using the available coordinates $\{x\}_i$ and velocities $\{v\}_i$ and the stochastic model defined by (15), the variation with respect to time of the original spatial orientation of the frame IGS08 were computed after implementing the least-squares procedure described in Section 3. The counterclockwise rotations $\delta\alpha_1, \delta\alpha_2, \delta\alpha_3$ and their uncertainties required to physically rotate the frame $\{x\}_i$ into $\{\tilde{x}\}_i$, triggering a new realization caused by the change in coordinates of the IGS08 stations due the rotation of the plates, were determined. The results are shown in Table 2 where the equivalence, 1 mas = 1 milliarcsecond = 0.001", has been used.

Table 2 Virtual secular motion of the IGS08 frame after applying to the 231 core stations defining this frame the observed plate velocities during a period of 50 years

Global Rotations		Secular Polar Motion IGS08	
$\delta\alpha_1$	-1.151 ± 1.798 (mas)	y_p	-0.036 ± 0.056 (m)
$\delta\alpha_2$	16.070 ± 1.809 (mas)	x_p	0.499 ± 0.056 (m)
$\delta\alpha_3$	-16.348 ± 1.954 (mas)	λ_p	-0.506 ± 0.060 (m)
$\Sigma_{\{\delta\alpha_1,\delta\alpha_2,\delta\alpha_3\}}$	$\begin{bmatrix} 3.2326 & -0.0688 & 0.4300 \\ -0.0688 & 3.2709 & 0.1370 \\ 0.4300 & 0.1370 & 3.8171 \end{bmatrix} (\text{mas}^2)$	$\Sigma_{\{y_p,x_p,\lambda_p\}}$	$\begin{bmatrix} 0.0031 & -0.0001 & 0.0004 \\ -0.0001 & 0.0031 & 0.0001 \\ 0.0004 & 0.0001 & 0.0036 \end{bmatrix} (\text{m}^2)$

$$\hat{\sigma}_0 = 1.3633; \quad \boldsymbol{\rho}_{\{\delta\alpha_1,\delta\alpha_2,\delta\alpha_3\}} = \boldsymbol{\rho}_{\{y_p,x_p,\lambda_p\}} = \begin{bmatrix} 1 & -0.0211 & 0.1224 \\ -0.0211 & 1 & 0.0388 \\ 0.1224 & 0.0388 & 1 \end{bmatrix}$$

Table 2 presents the values of the angular displacements of the original IGS08 frame after applying the displacements caused by the given secular velocities (mostly attributed to plate rotations) to the original coordinates of the stations during a period of 50 years. In order to better visualize these displacements in linear units, Figure 4 represents, using dashed lines, the secular magnitude and orientation of the displacements at the earth's pole and equator with

corresponding error ellipse and error bars. Recall that the variation of the IGS08 original frame is dependent on the selected core stations. To this restriction one should add the fact that the stations are located on different tectonic plates which rotate under various Euler rotation poles. Clearly, it is plausible to envisage an ideal combination of stations and plates that may provide the "best" definition of the frame. To dramatize this fact, in the following section the same theory and computational approach is applied when only the five IGS sites closest to the old ILS observatories are considered.

Results using only the five IGS08 stations which are closest to the former ILS astronomical observatories.

Table 1 shows the actual IGS08 stations closest to the old ILS observatories used. Notice that they are located between the band of north latitudes 36º 06' and 39º 58' and that only two plates are involved, the Eurasian plate (EU) and the North American plate (NA). Actually, Mizusawa is located in the confluence of the Eurasian plate with several microplates thus being very difficult to exactly ascertain to what plate this particular station belongs (see Figure 3).

Using only these five stations and the same least-squares procedure described before, the results of Table 3 were obtained. As expected, the secular rotations (or displacements) are not as well defined as before because only five stations, primarily located on only two different plates, are involved.

Table 3 Virtual secular motions of the IGS08 $\equiv$ ILS frame after applying to the five close-to-ILS stations the observed plate velocities during a period of 50 years

Global Rotations		Secular Polar Motion ILS	
$\delta\alpha_1$	12.408 $\pm$ 10.902 (mas)	y_p	0.385 $\pm$ 0.338 (m)
$\delta\alpha_2$	36.028 $\pm$ 11.952 (mas)	x_p	1.118 $\pm$ 0.371 (m)
$\delta\alpha_3$	-3.954 $\pm$ 11.490 (mas)	λ_p	-0.122 $\pm$ 0.355 (m)

$$\mathbf{\Sigma}_{\{\delta\alpha_1,\delta\alpha_2,\delta\alpha_3\}} \begin{bmatrix} 118.8636 & 1.6255 & 1.1446 \\ 1.6255 & 142.8604 & 3.7672 \\ 1.1446 & 3.7672 & 132.0274 \end{bmatrix} (\text{mas}^2) \quad \mathbf{\Sigma}_{\{y_p,x_p,\lambda_p\}} \begin{bmatrix} 0.1144 & 0.0016 & 0.0011 \\ 0.0016 & 0.1375 & 0.0036 \\ 0.0011 & 0.0036 & 0.1262 \end{bmatrix} (\text{m}^2)$$

$$\hat{\sigma}_0 = 0.6271; \ \mathbf{\rho}_{\{\delta\alpha_1,\delta\alpha_2,\delta\alpha_3\}} = \mathbf{\rho}_{\{y_p,x_p,\lambda_p\}} = \begin{bmatrix} 1 & 0.0125 & 0.0091 \\ 0.0125 & 1 & 0.0274 \\ 0.0091 & 0.0274 & 1 \end{bmatrix}$$

By comparing the results from Tables 2 and 3 it is evident that due to the difference in the number of stations used, the resultant v-c matrices of the modern more exhaustive and low-cost GPS methodology is, perceptibly, much more accurate that the classical astronomical procedure relying only on five observatories. That's why, in essence, the ILS organization was disbanded. The traditional astrometric techniques using zenith telescopes were replaced by new geodetic space methods, among them the GPS-based procedures which are the ones exclusively relied upon in this investigation.

The results are plotted in Figure 4 using the standard nomenclature and orientation of the x_p and y_p axes originally adopted by the ILS organization. The figure shows that the polar axis of the IGS08 frame will have a virtual secular motion of about 0.50 m in 50 years, practically along the zero-meridian, as a consequence of the displacement of the core stations defining the frame due largely to plate rotations. It is appropriate to note that this virtual secular motion of the pole will change depending on the selected stations and their location on the tectonic plates (fast moving vs slow moving). This is corroborated by the second example showed in the figure corresponding to the case where only the five ILS stations are considered. Notice that the direction and the magnitude of the displacement are different. The secular motion of the pole for the ILS case coincides very well with previous results published in Soler and Mueller (1978) that used modeled plate velocities that were introduced by Solomon et al. (1975). Of all the different plate models that these authors postulated to compute tectonic plate velocities the results presented here for the ILS stations coincide best with their model B4: continents have 3 times more drag than oceans. Recall that no accurate real measurements of tectonic plate rotations were available at that time. However, the newly determined error estimates of the computed direction and magnitude of the ILS inferred secular polar motion determined here encompasses

other models described in Solomon et al. (1975) (see Soler and Mueller 1978). Another related conclusion is that the detected virtual secular motion of the pole for a period of 50 years could not be attributed to glaciation effects and is mainly due to plate rotations. The glaciation hypothesis to explain the so-called wandering of the pole was commonly used before the global tectonic theory was introduced but although it may make sense for time periods of thousands of years it may not explain intervals of only 50 years as the one addressed in this exercise.

Furthermore, it is also plausible to assume that the historically detected small random changes in the direction of the path of the secular motion of the pole could be related, as Figure 4 implies, to the specific number of stations used at certain periods of time and their particular location on the tectonic plates. A more consistent average in the determination of the secular motion of the pole is obtained when the number of observing stations is increased and they are evenly distributed over the surface of the earth.

Recently, several scientific teams have produced tectonic plates velocity models based on observed geodetic and geophysical data, e.g. Goudarzi et al. 2014. The most comprehensive bibliographic information as well as the availability of handy Web-based plate calculators can be reached at the following URL:

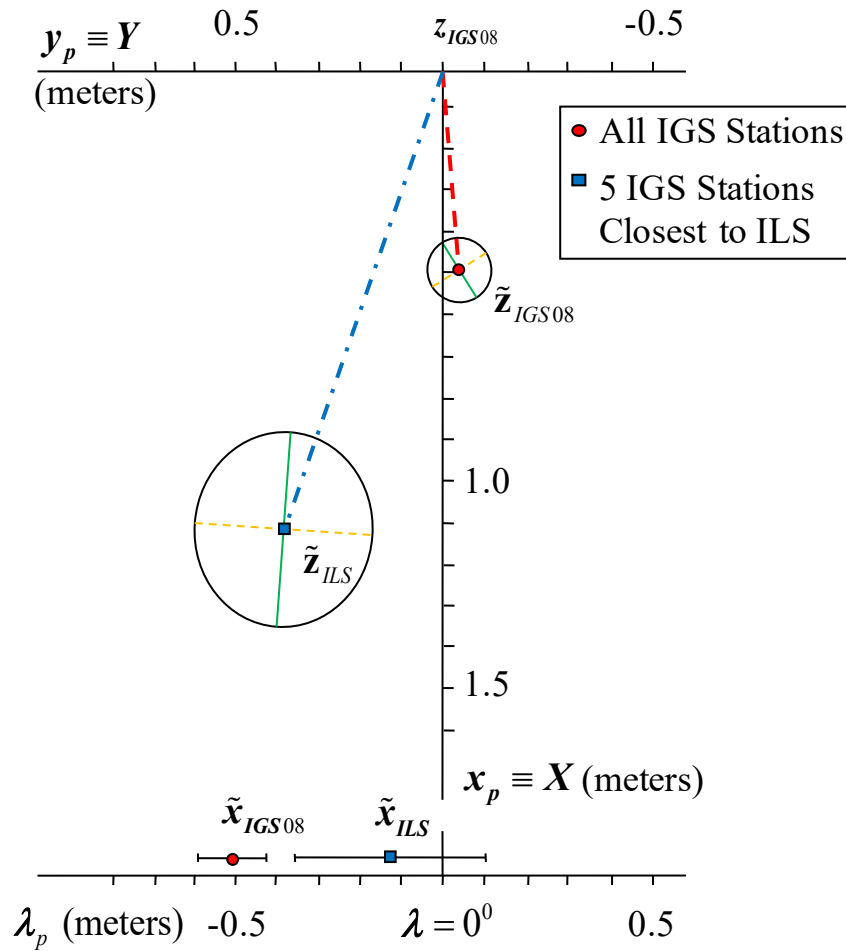http://www.unavco.org/community_science/science-support/crustal_motion/dxdt/model.html

Fig. 4 Displacements on the surface of the earth's ellipsoid of the pole z_{IGS08} and equatorial axis x_{IGS08} attributed to plate motions during a period of 50 years affecting the core 231 IGS08 and the 5 IGS/ILS-type stations

Effect of the secular motion of the frame on IGS08 core stations

Before proceeding further, a few points need to be clarified which otherwise could generate confusion when one mixes up in the same practical procedure rotation of frame axes (points remain fixed, frames move) and rotation of vectors (frame remains fixed, vector moves). This is also referred to in the literature as "passive" and "active" rotations, respectively (Soler 1998; Millot and Man 2012).

The authors believe that to avoid any possible misunderstandings when rotations are involved in any mathematical derivation the sign convention defining the rotations should be as consistent as possible. That is the main reason for selecting herein counterclockwise (anticlockwise) rotations of axes to be always positive. Therefore, every time that a rotation of an axis is performed, counterclockwise rotations are assumed positive. Consequently, the definition of the basic equation of a general rotation about an arbitrary axis needs to be addressed first as it is traditionally used in physics, and especially dynamics. The basic equations here refer to rotations of vectors, also referred to as active transformations or body rotations.

The formulation for active rotation of axis was originally introduced by Euler (1775) and revived a century later by Thomson and Tait (1879). In the abbreviated matrix notation of this work, the rotation matrix of the transformation takes the form:

$$\mathbf{R}_\ell(\alpha) = [1] + \sin\alpha\,[\underline{\ell}] + (1 - \cos\alpha)\,[\underline{\ell}]^2 \tag{24}$$

Notice that in (24) no assumption about the magnitude of α, the angle of rotation, was made, $0 \le \alpha \le 2\pi$. Furthermore, according to the matrix nomenclature advocated in this article the skew-symmetric matrix $[\underline{\ell}]$ is explicitly given by:

$$[\underline{\ell}] = \begin{bmatrix} 0 & -\ell_3 & \ell_2 \\ \ell_3 & 0 & -\ell_1 \\ -\ell_2 & \ell_1 & 0 \end{bmatrix} \tag{25}$$

Equation (24) represents a counterclockwise rotation of magnitude α about an axis of direction cosines ℓ_1, ℓ_2, ℓ_3. Assuming now that the angle of rotation is differentially small, equation (24) reduces to:

$$\mathbf{R}_\ell(\delta\alpha) = [1] + \sin\delta\alpha\,[\underline{\ell}] + (1 - \cos\delta\alpha)\,[\underline{\ell}]^2 = [1] + \delta\alpha\,[\underline{\ell}]$$

$$= [1] + \begin{bmatrix} 0 & -\delta\alpha_3 & \delta\alpha_2 \\ \delta\alpha_3 & 0 & -\delta\alpha_1 \\ -\delta\alpha_2 & \delta\alpha_1 & 0 \end{bmatrix} = [1] + [\underline{\delta\alpha}] = \begin{bmatrix} 1 & -\delta\alpha_3 & \delta\alpha_2 \\ \delta\alpha_3 & 1 & -\delta\alpha_1 \\ -\delta\alpha_2 & \delta\alpha_1 & 1 \end{bmatrix} \tag{26}$$

The final matrix in (26) is opposite in sign to (2) although both equations were derived assuming counterclockwise rotations positive. However, in (2) the rotations are taken about the

20

three Cartesian axes and the points remain fixed in space (see Figure 1), while in (26) the frame axes remain fixed and the vectors (points) are rotated (body rotation). Figure 5 depicts the parameters involved in a so-called active rotation.

Therefore, the transformation of the original coordinates $\{x\}_i$ referred to the frame (x, y, z) due to a counterclockwise differential rotation of magnitude $|\overrightarrow{\delta\alpha}| \equiv \delta\alpha$ around a vector $\overrightarrow{\delta\alpha}$ with components $(\delta\alpha_1, \delta\alpha_2, \delta\alpha_3)$ could be written:

$$\{x'\}_i = \mathbf{R}_\ell(\delta\alpha)\{x\}_i = [[1]+[\underline{\delta\alpha}]]\{x\}_i = \begin{Bmatrix} x \\ y \\ z \end{Bmatrix}_i + \begin{bmatrix} 0 & -\delta\alpha_3 & \delta\alpha_2 \\ \delta\alpha_3 & 0 & -\delta\alpha_1 \\ -\delta\alpha_2 & \delta\alpha_1 & 0 \end{bmatrix} \begin{Bmatrix} x \\ y \\ z \end{Bmatrix}_i \qquad (27)$$

and the differential contribution to the original coordinates $\{x\}_i$ caused by a counterclockwise rotation of vectors will be:

$$\begin{Bmatrix} \delta x \\ \delta y \\ \delta z \end{Bmatrix}_i = \begin{bmatrix} 0 & -\delta\alpha_3 & \delta\alpha_2 \\ \delta\alpha_3 & 0 & -\delta\alpha_1 \\ -\delta\alpha_2 & \delta\alpha_1 & 0 \end{bmatrix} \begin{Bmatrix} x \\ y \\ z \end{Bmatrix}_i = [\underline{\delta\alpha}]\{x\}_i \qquad (28)$$

The comparison of (2) and (28) summarizes conceptually the difference between differential counterclockwise rotation of axes and differential counterclockwise rotation of vectors, respectively. In most treatises of mechanics, the theory of rotations rotates the body (rotation of vectors, active rotations) as opposed to rotate the coordinate axes. Therefore, practically, equation (24) is used. This is also the case when plate tectonic rotations are invoked.

The rotation of coordinate axes started to be popularized at the dawn of the artificial satellite era when transformation between three-dimensional geodetic frames was originally postulated. The first serious investigation treating this particular subject was published by Lambeck (1971). This author, perhaps, to be consistent with the standards adopted by classical mechanics textbooks, selected counterclockwise rotation of axes as positive. This rotation convention remained unperturbed among geodesists until Boucher and Altamimi (1996), decided to switch the formulation used by the IERS to clockwise rotation of axes positive creating, in the process, confusion (see Soler 1997). Stressing further this point, the rotation of axes should be assumed counterclockwise positive to be consistent with a general body rotation about an arbitrary axis as

used today in dynamics and, particularly, by geophysicists investigating plate tectonic theories. Therefore, although both rotations are counterclockwise positive it is important to distinguish if the rotation is applied to the axes of a Cartesian frame (points remain fixed, Figure 1) or to vectors (frame remains fixed, Figure 5), because their matrix formulation is opposite in sign.
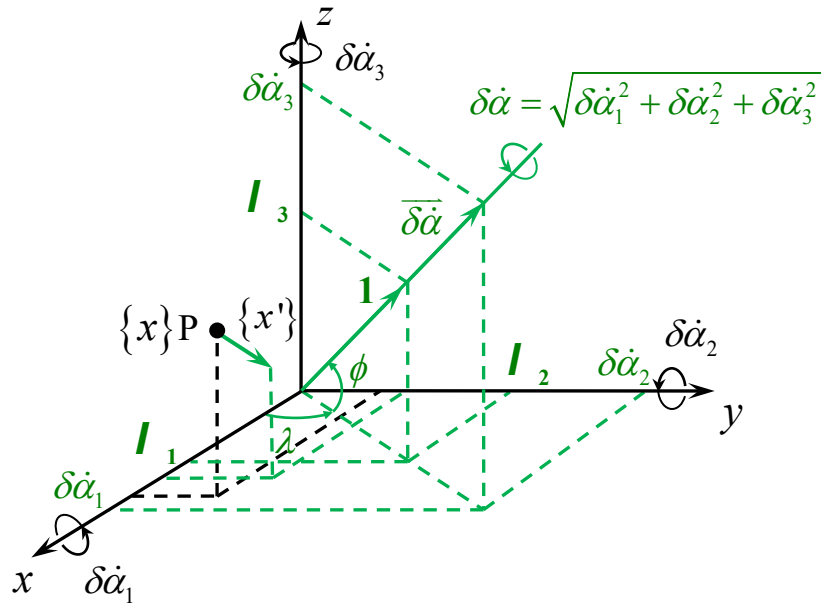

Fig. 5 Parameters defining Euler axis of rotation

Assume now that the IGS08 reference frame has a secular motion defined by the three counterclockwise rotations around the axes as derived from the results presented in Table 2. From the three counterclockwise rotations computed above caused by the individual plate velocities at each station for a period dt = 50 years, one immediately can determine the rates of the rotations according to:

$$\delta\alpha_1 = \text{-1.151 (mas)} \rightarrow \delta\dot\alpha_1 = \delta\alpha_1 / dt = \text{-0.0230 (mas/yr)}$$

$$\delta\alpha_2 = \text{16.070 (mas)} \rightarrow \delta\dot\alpha_2 = \delta\alpha_2 / dt = \text{0.3214 (mas/yr)} \qquad (29)$$

$$\delta\alpha_3 = \text{-16.348 (mas)} \rightarrow \delta\dot\alpha_3 = \delta\alpha_3 / dt = \text{-0.3270 (mas/yr)}$$

Remember that the above positive counterclockwise rotations were derived assuming rotations around the three axes. This could also be interpreted as an average "global" rotation that if

22

neglected could change with time the coordinates of the 231 IGS08 core stations. Clearly, this global rotation could be explained as the least-squares average secular rotation of the IGS08 frame resulting from the velocities of all stations, each one moving constrained by the rotation of the individual tectonic plate on which they are located.

Equation (28) could be converted into a dynamic-type equation by inserting the values of (29) and replacing the displacement of the coordinates by velocities, namely:

$$
\begin{Bmatrix} \dot{x} \\ \dot{y} \\ \dot{z} \end{Bmatrix}_i = \begin{bmatrix} 0 & -\delta\dot{\alpha}_3 & \delta\dot{\alpha}_2 \\ \delta\dot{\alpha}_3 & 0 & -\delta\dot{\alpha}_1 \\ -\delta\dot{\alpha}_2 & \delta\dot{\alpha}_1 & 0 \end{bmatrix} \begin{Bmatrix} x \\ y \\ z \end{Bmatrix}_i
\tag{30}
$$

Notice that the rotation is counterclockwise but now one is rotating vectors (active rotation). The above resulting velocities are referred to a local (topocentric) IGS08 Cartesian frame that could be transformed into a local (topocentric) geodetic frame east, north, up (e, n, u) as follows (Soler et al 2012):

$$
\begin{Bmatrix} \dot{e} \\ \dot{n} \\ \dot{u} \end{Bmatrix}_i = \mathbf{R}_i \begin{Bmatrix} \dot{x} \\ \dot{y} \\ \dot{z} \end{Bmatrix}_i = \begin{bmatrix} -\sin\lambda & \cos\lambda & 0 \\ -\cos\lambda\sin\varphi & -\sin\lambda\sin\varphi & \cos\varphi \\ \cos\lambda\cos\varphi & \sin\lambda\cos\varphi & \sin\varphi \end{bmatrix}_i \begin{Bmatrix} \dot{x} \\ \dot{y} \\ \dot{z} \end{Bmatrix}_i
\tag{31}
$$

The results of (31) for the ($\dot{e}, \dot{n}$) components referred to the local geodetic horizon plane are plotted at each point i in Figure 6.
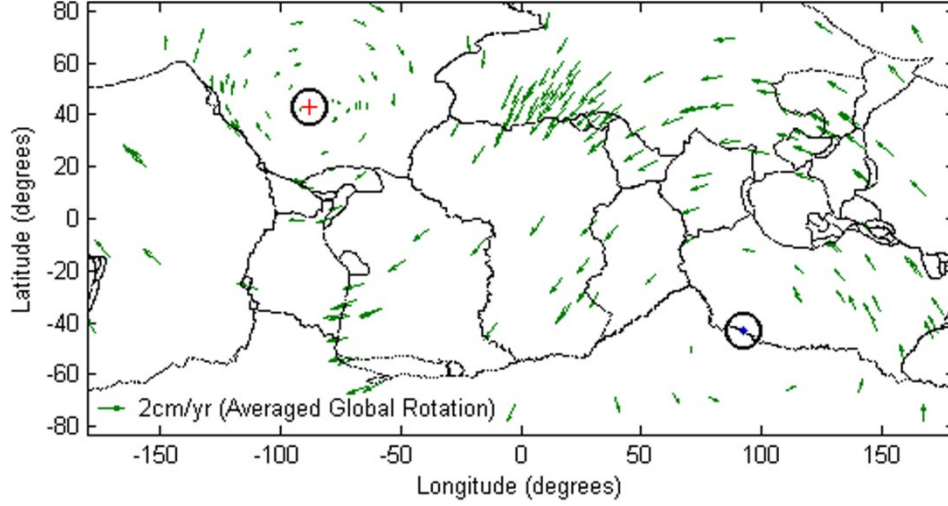
Fig. 6 Velocities at the 231 IGS08 stations caused by a global counterclockwise rotation of vectors of magnitude $\delta\dot\alpha$ and components $\delta\dot\alpha_1, \delta\dot\alpha_2, \delta\dot\alpha_3$. The two symbols indicate the top ⊡ and the tail $\oplus$ of the Euler vector axis

Exactly the same results for the velocities could be obtained using (27) in conjunction with the original coordinates, namely:

$$\{\dot x\}_i = (\{x'\}_i - \{x\}_i)/dt = \left(\mathbf{R}_\ell(\delta\alpha)\{x\}_i - \{x\}_i\right)/dt \tag{32}$$

where the rotation matrix $\mathbf{R}_\ell(\delta\alpha)$ could be computed using the general (24).

The spherical longitude and latitude of the Euler axis are determined as follows (see Figure 5):

$$\lambda = \arctan\left(\frac{\delta\alpha_2}{\delta\alpha_1}\right) = \arctan\left(\frac{\delta\dot\alpha_2}{\delta\dot\alpha_1}\right) \tag{33}$$

$$\phi = \arctan\left(\frac{\delta\alpha_3}{\sqrt{\delta\alpha_1^2 + \delta\alpha_2^2}}\right) = \arctan\left(\frac{\delta\dot\alpha_3}{\sqrt{\delta\dot\alpha_1^2 + \delta\dot\alpha_2^2}}\right) \tag{34}$$

and the angular rate of rotation:

$$\delta\dot\alpha = \frac{\delta\alpha}{dt} = \sqrt{\delta\dot\alpha_1^2 + \delta\dot\alpha_2^2 + \delta\dot\alpha_3^2} \tag{35}$$

The numerical values of λ, ϕ, and $\delta\dot\alpha$ in the above three equations, after inserting the quantities from Table 3, are presented in Table 4. The standard deviations of the two angles given the orientation of the Euler axis and the counterclockwise angular rotation rate $\delta\dot\alpha$ were obtained using the standard propagation of errors formulation, namely:

$$\Sigma_{\{\lambda,\phi,\delta\dot{\alpha}\}} = \begin{bmatrix} \sigma_\lambda^2 & \sigma_{\lambda\phi} & \sigma_{\lambda\delta\dot{\alpha}} \\ & \sigma_\phi^2 & \sigma_{\phi\delta\dot{\alpha}} \\ sym & & \sigma_{\delta\dot{\alpha}}^2 \end{bmatrix} = \underset{3\times3}{\mathbf{J}} \, \underset{3\times3}{\Sigma_{\{\delta\dot{\alpha}_1,\delta\dot{\alpha}_2,\delta\dot{\alpha}_3\}}} \, \mathbf{J}^T \tag{36}$$

where,

$$\mathbf{J} = \frac{\partial(\lambda,\phi,\delta\dot{\alpha})}{\partial(\delta\dot{\alpha}_1,\delta\dot{\alpha}_2,\delta\dot{\alpha}_3)} = \begin{bmatrix} -\dfrac{\delta\dot{\alpha}_2}{\delta\dot{\alpha}_1^2 + \delta\dot{\alpha}_2^2} & \dfrac{\delta\dot{\alpha}_1}{\delta\dot{\alpha}_1^2 + \delta\dot{\alpha}_2^2} & 0 \\[3mm] -\dfrac{\delta\dot{\alpha}_1\delta\dot{\alpha}_3}{\delta\dot{\alpha}^2\sqrt{\delta\dot{\alpha}_1^2 + \delta\dot{\alpha}_2^2}} & -\dfrac{\delta\dot{\alpha}_2\delta\dot{\alpha}_3}{\delta\dot{\alpha}^2\sqrt{\delta\dot{\alpha}_1^2 + \delta\dot{\alpha}_2^2}} & \dfrac{\sqrt{\delta\dot{\alpha}_1^2 + \delta\dot{\alpha}_2^2}}{\delta\dot{\alpha}^2} \\[3mm] \dfrac{\delta\dot{\alpha}_1}{\delta\dot{\alpha}} & \dfrac{\delta\dot{\alpha}_2}{\delta\dot{\alpha}} & \dfrac{\delta\dot{\alpha}_3}{\delta\dot{\alpha}} \end{bmatrix} \tag{37}$$

The positive intersection of the Euler's axis (the tip of the vector) with the surface of the earth is represented in Figure 6 by the symbol ⊡ while the tail of the vector is denoted by ⊕. Notice that the rotation, as usually defined, is counterclockwise positive.

Table 4 Euler Pole parameters with pertinent companion statistics

Euler Pole and Angular Rates	Size and Orientation of Error Ellipse
$\lambda = 94°\ 05'\ 53.6326" \pm 8°\ 42'\ 13.7950"$	$a_e = 8°\ 44'\ 6.6903" = 974.0126$ (km)
$\phi = -45°\ 25'\ 01.3227" \pm 6°\ 30'\ 8.8148"$	$b_e = 6°\ 27'\ 36.9342" = 718.0544$ (km)
$\delta\dot{\alpha} = 0.4591 \pm 0.0506$ (mas/yr)	$A_{a_e} = 97°\ 13'\ 32.5905"$

$$\Sigma_{\{\lambda,\phi,\delta\dot{\alpha}\}} = \begin{bmatrix} 75.7567 & -4.3135 & 0.0474 \\ -4.3135 & 42.2818 & -0.0250 \\ 0.0474 & -0.0250 & 0.0026 \end{bmatrix} \text{(deg}^2, \text{mas}^2/\text{yr}^2)$$

$$\rho_{\{\lambda,\phi,\delta\dot{\alpha}\}} = \begin{bmatrix} 1.0000 & -0.0762 & 0.1075 \\ -0.0762 & 1.0000 & -0.0761 \\ 0.1075 & -0.0761 & 1.0000 \end{bmatrix}$$

The standard formulation to compute in angular units the semi-major and –minor axes of the error ellipse was used. The angular units were converted into linear units according to the following equations:

$$\frac{1}{R_A} = \frac{\cos^2 A}{M} + \frac{\sin^2 A}{N} \Rightarrow R_A = \frac{MN}{N\cos^2 A + M\sin^2 A} \tag{38}$$

Where, R_A is the radius of curvature on the surface of the earth's ellipsoid along an azimuth A counted positive clockwise from the geodetic north.

The value of φ that should be used above to compute M and N as noted in (21) could be computed from the following equation:

$$\tan\varphi = \frac{\tan\phi}{1 - e^2} \tag{39}$$

Finally:

$$\underbrace{\begin{Bmatrix} a_e \\ b_e \end{Bmatrix}}_{\substack{linear \\ units}} = \begin{bmatrix} R_{\alpha_a} & 0 \\ 0 & R_{\alpha_b} \end{bmatrix} \underbrace{\begin{Bmatrix} a_e \\ b_e \end{Bmatrix}}_{radians} \tag{40}$$

The direction cosines of the Euler axis, if necessary, follow immediately from (Figure 5):

$$\begin{Bmatrix} \ell_1 \\ \ell_2 \\ \ell_3 \end{Bmatrix} = \begin{Bmatrix} \cos\phi\cos\lambda \\ \cos\phi\sin\lambda \\ \sin\phi \end{Bmatrix} = \begin{Bmatrix} -0.0502 \\ 0.7001 \\ -0.7122 \end{Bmatrix} \tag{41}$$

Considering that in this particular case the assumption is that the counterclockwise rotation of vectors is differentially small, then (32) simplifies as follows:

$$\{\dot{x}\}_i = (\{x'\}_i - \{x\}_i)/dt = \left(\mathbf{R}_\ell(\delta\alpha)\{x\}_i - \{x\}_i\right)/dt$$

$$= \left[[1]\{x\} + \sin\delta\alpha[\underline{\ell}]\{x\}_i - \underbrace{(1-\cos\delta\alpha)}_{\approx 0}[\underline{\ell}]^2\{x\}_i - \{x\}_i \right]/dt \tag{42}$$

$$= \delta\dot{\alpha}[\underline{\ell}]\{x\}_i = \begin{bmatrix} 0 & -\ell_3\delta\dot{\alpha} & \ell_2\delta\dot{\alpha} \\ \ell_3\delta\dot{\alpha} & 0 & -\ell_1\delta\dot{\alpha} \\ -\ell_2\delta\dot{\alpha} & \ell_1\delta\dot{\alpha} & 0 \end{bmatrix} \begin{Bmatrix} x \\ y \\ z \end{Bmatrix}_i = \begin{bmatrix} 0 & -\delta\dot{\alpha}_3 & \delta\dot{\alpha}_2 \\ \delta\dot{\alpha}_3 & 0 & -\delta\dot{\alpha}_1 \\ -\delta\dot{\alpha}_2 & \delta\dot{\alpha}_1 & 0 \end{bmatrix} \begin{Bmatrix} x \\ y \\ z \end{Bmatrix}_i$$

As expected, the above equation is identical to (30) found before. Thus, the global rotation generated by these three frame rotations could also be quantified by determining the longitude and latitude of an axis (Euler axis) going through the center of the earth and the magnitude of the angular rotation around this axis. Consequently, the velocities at any point caused by the rotation of a tectonic plate model could be calculated using two approaches depending of what type of parameters are given. If the variation with respect to time of the three components of the angular

rotation is given, then (30) could be used. If the longitude and latitude of the Euler's axis and the value of the angular rotation around this axis are known then the direction cosines approach also graphically displayed in Figure 5 should be implemented.

Alternative direct computation of the three Euler pole parameters

From (42) a new independent mathematical model could be established according to the following equation:

$$
\begin{Bmatrix} v_x \\ v_y \\ v_z \end{Bmatrix}_i = \begin{bmatrix} 0 & -\ell_3\delta\dot{\alpha} & \ell_2\delta\dot{\alpha} \\ \ell_3\delta\dot{\alpha} & 0 & -\ell_1\delta\dot{\alpha} \\ -\ell_2\delta\dot{\alpha} & \ell_1\delta\dot{\alpha} & 0 \end{bmatrix} \begin{Bmatrix} x \\ y \\ z \end{Bmatrix}_i \tag{43}
$$

Expressed, as before, in the form of mixed math model $F(X, L)=0$, after substituting the direction cosines from (41) above one can write the following functional relationships:

$$
\begin{aligned}
F_1 :\ & v_{x_1} + \sin\phi\,\delta\dot{\alpha}\,y_1 - \cos\phi\sin\lambda\,\delta\dot{\alpha}\,z_1 = 0 \\
F_2 :\ & v_{y_1} - \sin\phi\,\delta\dot{\alpha}\,x_1 + \cos\phi\cos\lambda\,\delta\dot{\alpha}\,z_1 = 0 \\
F_3 :\ & v_{z_1} + \cos\phi\sin\lambda\,\delta\dot{\alpha}\,x_1 - \cos\phi\cos\lambda\,\delta\dot{\alpha}\,y_1 = 0 \\
& \qquad\qquad \vdots \\
F_{3n-2} :\ & v_{x_n} + \sin\phi\,\delta\dot{\alpha}\,y_n - \cos\phi\sin\lambda\,\delta\dot{\alpha}\,z_n = 0 \\
F_{3n-1} :\ & v_{y_n} - \sin\phi\,\delta\dot{\alpha}\,x_n + \cos\phi\cos\lambda\,\delta\dot{\alpha}\,z_n = 0 \\
F_{3n} :\ & v_{z_n} + \cos\phi\sin\lambda\,\delta\dot{\alpha}\,x_n - \cos\phi\cos\lambda\,\delta\dot{\alpha}\,y_n = 0
\end{aligned} \tag{44}
$$

Then, according to (10) considering that now the parameters are $p_1 = \lambda$, $p_2 = \phi$, and $p_3 = \delta\dot{\alpha}$, the design matrix $\mathbf{A}$ will be given explicitly by the expression:

$$
\underset{3n\times3}{\mathbf{A}} = \left.\frac{\partial F}{\partial X}\right|_{X_0, L_b} =
$$

$$
=\begin{bmatrix}
\begin{bmatrix}
-\cos\phi\cos\lambda\,\delta\dot\alpha\,z_1 & \cos\phi\,\delta\dot\alpha\,y_1 + \sin\phi\sin\lambda\,\delta\dot\alpha\,z_1 & \sin\phi\,y_1 - \cos\phi\cos\lambda\,z_1 \\
-\cos\phi\sin\lambda\,\delta\dot\alpha\,z_1 & -\cos\phi\,\delta\dot\alpha\,x_1 - \sin\phi\cos\lambda\,\delta\dot\alpha\,z_1 & -\sin\phi\,x_1 + \cos\phi\cos\lambda\,z_1 \\
\cos\phi\cos\lambda\,\delta\dot\alpha\,x_1 + \cos\phi\sin\lambda\,\delta\dot\alpha\,y_1 & -\sin\phi\sin\lambda\,\delta\dot\alpha\,x_1 + \sin\phi\cos\lambda\,\delta\dot\alpha\,y_1 & \cos\phi\sin\lambda\,x_1 - \cos\phi\cos\lambda\,y_1
\end{bmatrix} \\
\vdots \\
\vdots \\
\begin{bmatrix}
-\cos\phi\cos\lambda\,\delta\dot\alpha\,z_n & \cos\phi\,\delta\dot\alpha\,y_n + \sin\phi\sin\lambda\,\delta\dot\alpha\,z_n & \sin\phi\,y_n - \cos\phi\cos\lambda\,z_n \\
-\cos\phi\sin\lambda\,\delta\dot\alpha\,z_n & -\cos\phi\,\delta\dot\alpha\,x_n - \sin\phi\cos\lambda\,\delta\dot\alpha\,z_n & -\sin\phi\,x_n + \cos\phi\cos\lambda\,z_n \\
\cos\phi\cos\lambda\,\delta\dot\alpha\,x_n + \cos\phi\sin\lambda\,\delta\dot\alpha\,y_n & -\sin\phi\sin\lambda\,\delta\dot\alpha\,x_n + \sin\phi\cos\lambda\,\delta\dot\alpha\,y_n & \cos\phi\sin\lambda\,x_n - \cos\phi\cos\lambda\,y_n
\end{bmatrix}
\end{bmatrix}
$$

(45)

Similarly, the design matrix $\mathbf{B}$ is given by:

$$
\mathbf{B}_{3n\times 6n} = \left.\frac{\partial F}{\partial L}\right|_{X_0,L_b} =
$$

$$
\begin{bmatrix}
\begin{bmatrix}
0 & \sin\phi\,\delta\dot\alpha & -\cos\phi\sin\lambda\,\delta\dot\alpha & 1 & 0 & 0 \\
-\sin\phi\,\delta\dot\alpha & 0 & \cos\phi\cos\lambda\,\delta\dot\alpha & 0 & 1 & 0 \\
\cos\phi\sin\lambda\,\delta\dot\alpha & -\cos\phi\cos\lambda\,\delta\dot\alpha & 0 & 0 & 0 & 1
\end{bmatrix}_1 & \cdots & \begin{bmatrix}
0 & 0 & 0 & 0 & 0 & 0 \\
0 & 0 & 0 & 0 & 0 & 0 \\
0 & 0 & 0 & 0 & 0 & 0
\end{bmatrix} \\
\vdots & \ddots & \vdots \\
\begin{bmatrix}
0 & 0 & 0 & 0 & 0 & 0 \\
0 & 0 & 0 & 0 & 0 & 0 \\
0 & 0 & 0 & 0 & 0 & 0
\end{bmatrix} & \cdots & \begin{bmatrix}
0 & \sin\phi\,\delta\dot\alpha & -\cos\phi\sin\lambda\,\delta\dot\alpha & 1 & 0 & 0 \\
-\sin\phi\,\delta\dot\alpha & 0 & \cos\phi\cos\lambda\,\delta\dot\alpha & 0 & 1 & 0 \\
\cos\phi\sin\lambda\,\delta\dot\alpha & -\cos\phi\cos\lambda\,\delta\dot\alpha & 0 & 0 & 0 & 1
\end{bmatrix}_n
\end{bmatrix}
$$

(46)

The closure vector $\mathbf{W}$ follows immediately from (44) and will not be given here explicitly. Using the same weight matrix as before, after implementing (17), (18), and (19), the results presented in Table 5 were obtained. The solution converged after five iterations. Comparing Table 4 to Table 5 shows that, as expected, the results are identical to the order of 0.0001 mas, except for the signs of the covariances that depend on the angular rotation rate parameter $\delta\dot\alpha$ which have opposite signs. Recall that both rotations are counterclockwise positive but one is a rotation of frames (passive rotation) and the other is an active rotation (body rotation).

This difference in sign of these covariances could be succinctly explained as follows. In the least-squares solution of model 1, positive counterclockwise rotations around the three axes of the IGS frame were assumed. Therefore, the frame was rotated and using (35) the value of $\delta\dot\alpha$ was computed. For clarity, let us introduce now the notation $\delta\dot\alpha_F$ where the subindex F indicates

"frame rotation." In the LS solution of model 2 the angular rotation rate around the Euler axis was also assumed counterclockwise positive. However, in this particular instance a "rotation of vectors" denoted now $\delta\dot{\alpha}_V$ was performed instead of a rotation of frames.

Although both rotations are counterclockwise positive, as explained above, they are opposite in sign; in other words a counterclockwise rotation of frames is equal to a negative clockwise rotation of frames or, equivalently, a negative counterclockwise rotation of vectors. Therefore, for all practical purposes, symbolically one can write: $\delta\dot{\alpha}_V = -\delta\dot{\alpha}_F$ leading to the following conceptual equation:

$$\left.\begin{array}{c} propagation \ \ of \ \ errors \\ from \ \ LS \ \ results, \ \ MODEL \ \ 1 \end{array}\right\} \left\{\begin{array}{c} \sigma_{\lambda_F \delta\dot{\alpha}_F} \\ \sigma_{\phi_F \delta\dot{\alpha}_F} \end{array}\right\} = \left\{\begin{array}{c} -\sigma_{\lambda_V \delta\dot{\alpha}_V} \\ -\sigma_{\phi_V \delta\dot{\alpha}_V} \end{array}\right\} \left\{\begin{array}{c} direct \ \ v-c \ \ matrix \\ from \ \ LS \ \ results, \ \ MODEL \ \ 2 \end{array}\right. \tag{47}$$

The argument elaborated before and the above definition should suffice to explain the reasons for the difference in sign of the covariances described in (47). Nevertheless, for completeness a more rigorous mathematical derivation follows. Our primary aim is to obtain the v-c matrix $\mathbf{\Sigma}_{\{\lambda_F,\phi_F,\delta\dot{\alpha}_F\}}$ as a function of the "truth" which it is assumed to be the v-c matrix obtained through the rigorous LS process, mainly, $\mathbf{\Sigma}_{\{\lambda_V,\phi_V,\delta\dot{\alpha}_V\}}$.

The functional relationship is this case could be written:

$$\left\{\begin{array}{l} \lambda_F = \lambda_V \\ \phi_F = \phi_V \\ \delta\dot{\alpha}_F = -\delta\dot{\alpha}_V \end{array}\right. \tag{48}$$

Then, one can solve the problem, by simple propagation of errors:

$$\mathbf{\Sigma}_{\{\lambda_F,\phi_F,\delta\dot{\alpha}_F\}} = \underset{3\times3}{\mathbf{J}} \ \mathbf{\Sigma}_{\{\lambda_V,\phi_V,\delta\dot{\alpha}_V\}} \ \underset{3\times3}{\mathbf{J}^T} \tag{49}$$

And the required Jacobian matrix is given explicitly by:

$$\mathbf{J} = \frac{\partial(\lambda_F,\phi_F,\delta\dot{\alpha}_F)}{\partial(\lambda_V,\phi_V,\delta\dot{\alpha}_V)} = \begin{bmatrix} 1 & 0 & 0 \\ 0 & 1 & 0 \\ 0 & 0 & -1 \end{bmatrix} \tag{50}$$

Therefore, immediately follows:

$$
\begin{bmatrix} \sigma^2_{\lambda_F} & \sigma_{\lambda_F \phi_F} & \sigma_{\lambda_F \delta\dot\alpha_F} \\ & \sigma^2_{\phi_F} & \sigma_{\phi_F \delta\dot\alpha_F} \\ sym & & \sigma^2_{\delta\dot\alpha_F} \end{bmatrix} = \boldsymbol{J} \begin{bmatrix} \sigma^2_{\lambda_V} & \sigma_{\lambda_V \phi_V} & \sigma_{\lambda_V \delta\dot\alpha_V} \\ & \sigma^2_{\phi_V} & \sigma_{\phi_V \delta\dot\alpha_V} \\ sym & & \sigma^2_{\delta\dot\alpha_V} \end{bmatrix} \boldsymbol{J}^T = \begin{bmatrix} \sigma^2_{\lambda_V} & \sigma_{\lambda_V \phi_V} & -\sigma_{\lambda_V \delta\dot\alpha_V} \\ & \sigma^2_{\phi_V} & -\sigma_{\phi_V \delta\dot\alpha_V} \\ sym & & \sigma^2_{\delta\dot\alpha_V} \end{bmatrix} \quad (51)
$$

which proves the mathematical statement made in (47).

Table 5 Euler Pole parameters with pertinent companion statistics

Euler Pole and Angular Rates	Size and Orientation of Error Ellipse
$\lambda = 94°\ 05'\ 53.6326'' \pm 8°\ 42'\ 13.7950''$	$a_e = 8°\ 44'\ 6.6903'' = 974.0126\ (km)$
$\phi = -45°\ 25'\ 01.3227'' \pm 6°\ 30'\ 8.8148''$	$b_e = 6°\ 27'\ 36.9342'' = 718.0544\ (km)$
$\delta\dot\alpha = 0.4591 \pm 0.0506\ (mas/yr)$	$A_{a_e} = 97°\ 13'\ 32.5905''$

$$
\boldsymbol{\Sigma}_{\{\lambda,\phi,\delta\dot\alpha\}} = \begin{bmatrix} 75.7567 & -4.3135 & -0.0474 \\ -4.3135 & 42.2818 & 0.0250 \\ -0.0474 & 0.0250 & 0.0026 \end{bmatrix} (deg^2, mas^2/yr^2)
$$

$$
\boldsymbol{\rho}_{\{\lambda,\phi,\delta\dot\alpha\}} = \begin{bmatrix} 1.0000 & -0.0762 & -0.1075 \\ -0.0762 & 1.0000 & 0.0761 \\ -0.1075 & 0.0761 & 1.0000 \end{bmatrix}
$$

Global rotation effect on the computed plate velocities.

As a consequence of the discussion elaborated above, it appears that an average global secular motion of the axes of the IGS08 frame is induced by the effect of the velocities at each one of the 231 points defining the frame which is caused by the rotation of the tectonic plates. Assume that the definition of the IGS08 frame is not significantly altered in a 50 year period because a correction has been applied to the observed coordinates to bring them back to the original epoch 2005.00. However, the observed velocities that were used to apply this correction may have implicit a contribution due to the virtual global secular motion of the frame discussed above and depicted in Figure 6. This concept of adding secular contributions to the velocities of points on

the earth's surface is not new. Recently Booker et al. (2014) entertained this idea writing explicitly: "The secular motion of any point on the earth will be a combination of GIA, plate tectonics, present-day surface mass loading, and other secular effects which we here assume to be negligible." Clearly, the secular motion of the frame itself as described herein could be another contribution not to be discarded. Consequently, in our opinion, a part of the GPS-observed velocities comprises the effect of a secular global rotation of the frame. To graphically clarify this argument Figure 7 depicts the three vector velocities involved at any arbitrary point P, from which easily follows:

IGS08 (observed plate rotation vector) = True plate rotation + global rotation   (52)

Therefore:

True plate rotation = IGS08 (observed plate rotation vector) - global rotation   (53)

   For completeness, the IGS08 observed plate rotation velocities available from the IGS08 SINEX file are depicted in Figure 8.
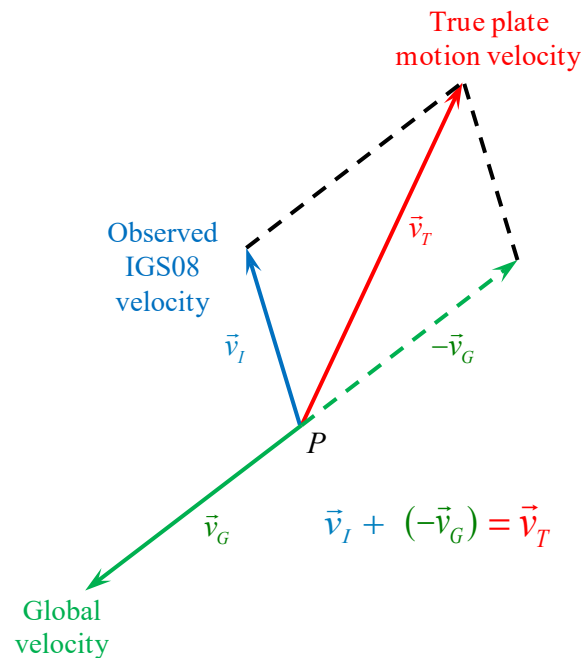

Fig. 7 Final true plate velocity resulting from the global rotation velocity and IGS08 observed plate velocities
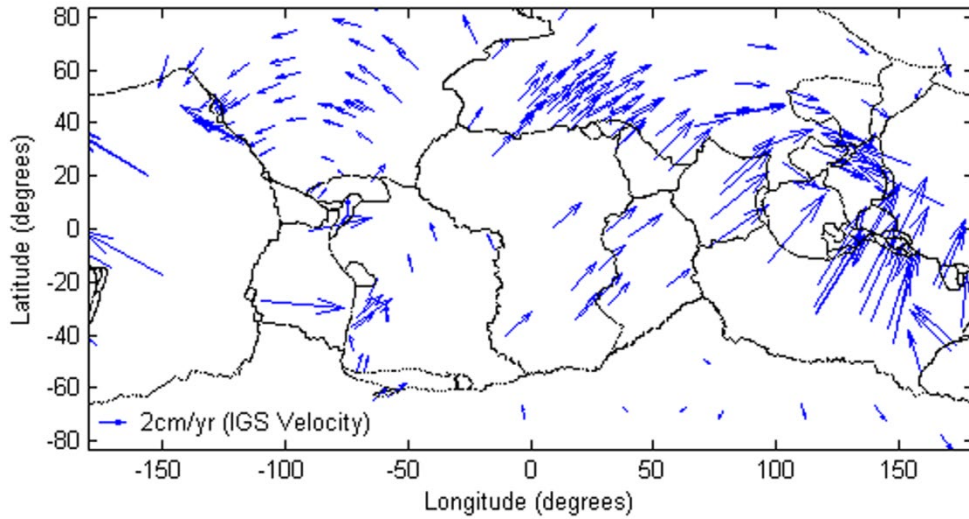
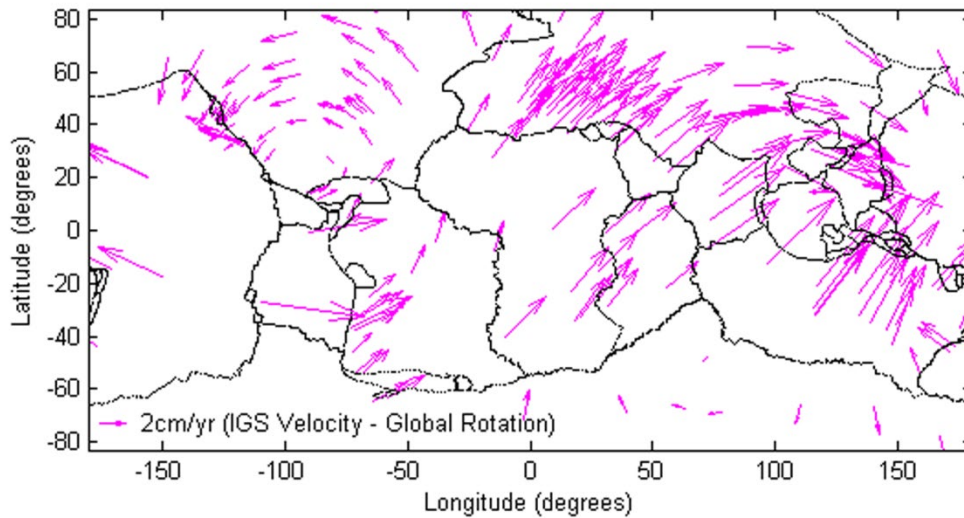**Fig. 8** Original GPS-determined IGS08 velocities from SINEX file

Fig. 9 True plate velocities (Difference between IGS08 velocities and the velocities caused by a secular rotation of the frame)

Implementing (53) one arrives to the vectors shown in Figure 9. Because the effect of the global rotation (Figure 6) is generally opposite in sign to the IGS08 observed velocities the combined outcome results in a real plate velocity that is larger than the observed one (Figs. 7 and 9). In other words, the true velocities at the stations once the global rotation effect is taken into consideration are usually larger than the observed ones.

To visualize approximately by how much the true plate velocities are larger or smaller than the observed values, Table 6 was constructed. All important tectonic plates are named by the two

letter acronym conventionally used in the geophysical literature and they are listed alphabetically in the first column of the table. The second column indicates the number of stations from the set of IGS08 core stations that belong to each particular plate. The 3rd and 4th columns are the averages of the east and north IGS08 observed velocity components within each plate, namely:

$$v_{e_I} = \frac{\sum_{i=1}^{m} v_{e,i}}{m}; \quad v_{n_I} = \frac{\sum_{i=1}^{m} v_{n,i}}{m} \quad (m = \text{number of stations in that plate}) \tag{54}$$

The fifth column is the averaged magnitude of the IGS08 velocity (on the local horizon plane) corresponding to each plate computed as follows:

$$v_I = \frac{\sum_{i=1}^{m} v_i}{m} = \frac{\sum_{i=1}^{m} \sqrt{v_{e_I,i}^2 + v_{n_I,i}^2}}{m} \tag{55}$$

The same logic was applied to compute the values in the 6th, 7th, and 8th columns corresponding to the components and magnitudes of the global velocities v_G.

The 9th column is the averaged magnitude of the "true" velocity, the difference between the IGS08 observed and global based on the following equation:

$$\text{True vel.} = v_T = \frac{\sum_{i=1}^{m} \delta v_i}{m} = \frac{\sum_{i=1}^{m} \sqrt{(\delta v_{e,i})^2 + (\delta v_{n,i})^2}}{m} \tag{56}$$

where $\delta v_{e,i} = v_{e_{I_i}} - v_{e_{G_i}}$ and $\delta v_{n,i} = v_{n_{I_i}} - v_{n_{G_i}}$ are the difference between the IGS08 and global east and north velocity components at each station within that plate, respectively. The last column of Table 6 shows the difference between the average value of the computed true and IGS08 velocities for each plate, v_T -v_I . Notice that while for the North American plate (45 stations) the true average value of the true velocity is only 3 mm/yr larger than the IGS08 observed value, for the European plate (63 stations) the average true value is 1.25 cm/yr larger than the IGS08 observed value. The results show a perceptible correlation between the values v_T -v_I and the magnitude of the average velocity for each plate. Summarizing, neglecting the contribution of the global induced rotation as postulated in this investigation, according to the results of Table 6, may introduce an error in the value of the true plate rotation velocities of the

major plates (number of points above 10 stations) between a maximum of 1.25cm/yr (EU plate) and a minimum of -1.06cm/yr (PA plate). Consequently, proper adjustment for the effect of the secular global rotation should be incorporated into the procedure used to compute GPS-observed point displacements to rigorously determine true plate rotation velocities.

Table 6 The averaged IGS08 and global velocities in each tectonic plate. Final discrepancies between averaged "true" and observed velocities at the major plates

Plate ID	Number of stations	IGS velocities (cm/yr)			Global velocities (cm/yr)			True vel.	$v_T - v_I$ (cm/yr)
		v_{e_I}	v_{n_I}	v_I	v_{e_G}	v_{n_G}	v_G	v_T (cm/yr)	
AF	15	1.84	1.86	2.62	-0.80	-0.94	1.24	3.85	1.23
AM	5	2.60	-1.21	2.87	-1.31	0.50	1.41	4.28	1.41
AN	11	0.51	0.02	1.12	-0.21	-0.22	0.89	1.83	0.71
AR	3	2.98	2.74	4.05	-1.19	-0.72	1.40	5.42	1.37
AT	2	1.03	1.36	1.84	-1.10	-0.87	1.40	3.14	1.30
AU	20	2.98	5.38	6.23	-0.61	0.59	0.90	6.04	-0.19
CA	3	0.80	0.90	1.20	-0.74	-0.10	0.77	1.86	0.66
EU	63	2.21	1.18	2.65	-0.91	-0.74	1.27	3.90	1.25
IN	4	4.28	3.53	5.55	-1.18	-0.30	1.22	6.67	1.12
MA	2	-0.92	0.48	1.04	-1.13	0.77	1.37	0.36	-0.68
NA	45	-1.39	-0.10	1.74	-0.01	0.09	0.52	2.04	0.30
ND	2	0.33	1.35	1.44	-0.98	-0.17	0.99	2.06	0.62
NZ	4	5.92	0.22	5.98	-1.17	0.24	1.20	7.15	1.17
OK	4	-0.36	-0.69	0.78	-1.16	0.76	1.39	1.68	0.90
ON	2	2.61	-2.06	3.32	-1.27	0.59	1.41	4.70	1.38
PA	18	-5.01	2.95	5.90	-0.73	0.85	1.13	4.84	-1.06
PS	1	-3.67	1.22	3.87	-1.20	0.74	1.41	2.52	-1.35
SA	14	0.48	1.28	1.60	-1.28	-0.44	1.38	2.59	0.99
SB	1	2.76	5.29	5.97	-0.93	0.79	1.22	5.82	-0.15
SO	6	2.17	1.65	2.74	-0.84	-0.82	1.18	3.91	1.17
SU	1	-2.91	0.64	2.98	-1.20	0.45	1.28	1.72	-1.26
YA	5	3.13	-1.16	3.33	-1.31	0.43	1.38	4.71	1.38
Mean		1.02	1.22	3.13	-0.97	0.07	1.20	3.69	0.56
Std. dev.		2.62	1.91	1.80	0.35	0.62	0.24	1.85	0.05

Conclusions

This investigation deliberately attempted to contrast rotations around frame axes with rotations of physical geocentric positional vectors with the intention of clarifying some common

misunderstandings that arise when both types of rotations (passive and active) are simultaneously combined. It was postulated that the rotation of tectonic plates may induce a global virtual rotation of any frame defined by the coordinates of a set of stations located on the moving earth's lithospheric plates. A component of this global secular rotation could be associated with a motion of the geodetic frame third axes (secular polar motion). After a least-squares procedure was devised and implemented, it was determined that the global rotation of the frame caused by displacement of the observing stations due to tectonic plate rotations causes a secular motion of the pole whose magnitude and direction is directly related to the number of stations and their location on each particular plate (e.g. slow moving vs fast moving). This supposition was clarified after results obtained when using five IGS sites close to the original five observatories of the now defunct International Latitude Service (ILS), was contrasted with the latest full set of stations defining the IGS08 geodetic frame. This one-to-one comparison shows significant differences in the two solutions and their resultant v-c matrices. Furthermore, it appears that neglecting the contribution of the secular global rotation in the determination of observed plate rotation velocities may distort the final interpretation of the plate velocities themselves. The outcome of this exercise suggests that the global rotation of the geodetic frame should be considered when an accurate determination of plate velocities is intended. GPS technological advancements and procedures are currently so accurate that the contribution of the as yet concealed secular motion of the frame in the determination of plate velocities should not be totally discarded.

References

Booker D, Clark PJ, Lavallée DA (2014) Secular changes in Earth's shape and surface mass loading derived from combination of reprocessed global GPS network. J Geod 88:839-855

Boucher C, Altamimi Z (1996) International terrestrial reference frame. GPS World 7(9):71-74

Euler L (1775) Nova methodus motum corporum rigidorum determinandi. Novi Commentari Academiae Scientiarum Imperialis Petropolitanae 20, 208-238. Reprinted in 1868. Opera Omnia (2) 9, 99-125, Societatis Scientiarum Naturalium Helveticae, Basileae

Höpfner J (2000) The International Latitude Service–A historical review, from the beginning to its foundation in 1899 and the period until 1922. Surveys Geophys 21:521-566

Goudarzi MA, Cocard M, Santerre R (2014) EPC: Matlab software to estimate Euler pole parameters. GPS Sol 18(1):153-162

Kaula WM (1966) Theory of Satellite Geodesy. Blaisdell Publishing Co., Waltham, Mass

Lambeck K (1971) The relation of some geodetic datums to a global geocentric reference system. Bull Géod (continued as J Geod) 99(1):37-53

Leick A (1995) GPS satellite surveying, 2nd edn. Wiley, New York, NY

McCarthy DD, Luzum BJ (1996) Path of the mean rotational pole from 1899 to 1994. Geophys J Int 125:623-629

Millot Y, Man PP (2012) Active and passive rotations with Euler angles in NMR. Concepts Magn Reson 40A: 215-252. Doi:10.1002/cmr.a.21242

Moritz H (1992) Geodetic reference system 1980. Bull Géod (continued as J Geod) 66(2):187-192

Mueller II (1969) Spherical and practical astronomy applied to geodesy. Frederic Ungar Publishing Co., New York, NY

Petit G, Luzum B (eds.) (2010) IERS Conventions (2010) IERS Technical Note No. 36. Verlag des Bundesamts für Kartographie und Geodäsie, Frankfurt am Main, Germany

Soler T (1997) Arbitrary alterations. GPS World 8(2):12

Soler T (1998) A compendium of transformation formulas useful in GPS work. J Geod 72(7-8): 482-490

Soler T, Han JY, Weston ND (2012) Alternative transformation from Cartesian to geodetic coordinates by least squares for GPS georeferencing applications. Comp & Geosci 42:100-109

Soler T, Mueller II (1978) Global plate tectonics and the secular motion of the pole. Bull Géod (continued as J Geod) 52(1):39-57

Solomon SC, Sleep NH, Richardson RM (1975) Forces driving plate tectonics: Inferences from absolute plate velocities and intraplate stress. Geophys J R astron Soc 42(2):769-801

Thomson W (Lord Kelvin), Tait PG (1879) Principles of mechanics and dynamics (formerly titled Treatise on natural philosophy), Part one. Cambridge University Press, Cambridge. Reprinted in 1944. Dover Publication, New York

Yokoyama K, Manabe S, Sakai S (2000) History of the International Polar Motion Service/International Latitude Service in Polar Motion: Historical and Scientific Problems. ASP Conference Series, 208, Dick S, McCarthy D, Luzum B (eds.), 147-162